Enhanced removal of acid orange II from aqueous solution by V and N co-doping TiO_2-MWCNTs/γ-Al_2O_3 composite photocatalyst induced by pulsed discharge plasma

Guangzhou Qu, Hui Wang, Xin Li, Tiecheng Wang, Zengqiang Zhang, Dongli Liang and Hong Qiang

ABSTRACT

This paper presents a study of V and N co-doping TiO_2 embedding multi-walled carbon nanotubes (MWCNTs) supported on γ-Al_2O_3 pellet (V/N-TiO_2-MWCNTs/γ-Al_2O_3) composite photocatalyst induced by pulsed discharge plasma to enhance the removal of acid orange II (AO7) from aqueous solution. The photocatalytic activity of the V/N-TiO_2-MWCNTs/γ-Al_2O_3 composite to AO7 removal induced by the pulsed discharge plasma was evaluated. The results indicate that the V/N-TiO_2-MWCNTs/γ-Al_2O_3 composite possesses enhanced photocatalytic activity that facilitates the removal of AO7 compared with the TiO_2-MWCNTs/γ-Al_2O_3 and TiO_2/γ-Al_2O_3 composites. Almost 100% of AO7 is removed after 10 min under optimal conditions. The $V_{0.10}$/$N_{0.05}$-TiO_2-MWCNTs/γ-Al_2O_3 photocatalyst exhibits the best removal effect for AO7. Analysis of the removal mechanism indicates that the enhancement of the removal of AO7 resulting from V and N co-doping causes TiO_2 lattice distortion and introduces a new impurity energy level, which not only reduces the band gap of TiO_2 but also inhibits the recombination of the e^-_{cb}/h^+_{vb} pairs.

Key words | azo dye, co-doping, pulsed discharge plasma, removal mechanism, TiO_2-MWCNTs

Guangzhou Qu (corresponding author)
Hui Wang
Xin Li
Tiecheng Wang
Zengqiang Zhang
Dongli Liang
Hong Qiang
College of Natural Resources and Environment,
Northwest A&F University,
Yangling, Shaanxi, 712100,
China
E-mail: *qugz@nwsuaf.edu.cn*

Guangzhou Qu
Tiecheng Wang
Zengqiang Zhang
Dongli Liang
Hong Qiang
Key Laboratory of Plant Nutrition and the Agri-environment in Northwest China,
Ministry of Agriculture,
Yangling, Shaanxi, 712100,
China

HIGHLIGHTS

- An efficient and easily recycled V/N-MWCNTs-TiO_2/ γ-Al_2O_3 composite was prepared.
- Activity of the composite induced by discharge plasma to AO7 removal was evaluated.
- Synergistic effect of discharge plasma and catalyst effectively improve AO7 removal.
- The composite demonstrates adequate recycling performance in a discharge plasma system.
- Possible mechanisms of AO7 removal were analyzed.

doi: 10.2166/wst.2020.579

GRAPHICAL ABSTRACT

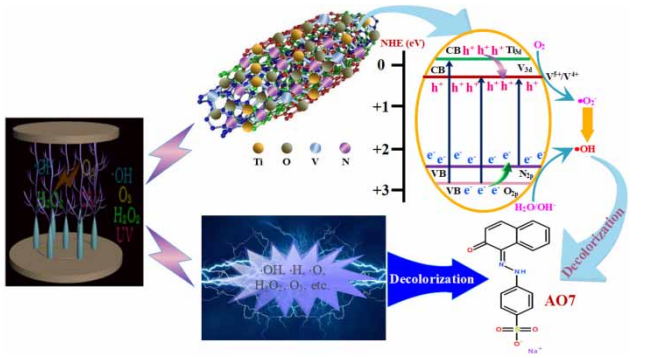

INTRODUCTION

Pulsed discharge plasma technology has been widely studied as one of several advanced oxidation processes in the treatment of persistent liquid phase organic pollutants, specifically in the decolorization of textile dye wastewater (Jiang *et al.* 2014). It not only directly generates oxidizing species (such as ·OH, ·O, H_2O_2 and O_3) during the discharge process but also with physical effects, such as ultraviolet (UV) light, strong electric fields, electro-hydraulic cavitations and supercritical water oxidation, etc. (Joshi *et al.* 1995; Locke *et al.* 2006; Jiang *et al.* 2012). However, the physical properties, especially for light, are not fully utilized for the degradation of pollutants. If the physical effects that possess parts of the discharge energy could also be utilized for the degradation of pollutants, an enhancement of the removal rate of the pollutants and the utilization rate of the discharge energy could be realized.

TiO_2, as a good photocatalytic material, has been extensively studied in the last two decades due to its potential as a low cost, non-toxic, highly efficient and stable photocatalyst under UV light irradiation (Murthy *et al.* 2017). Fujishima *et al.* (2000) indicated that even a few photons (i.e. as low as 1 $\mu W \cdot cm^{-2}$) can be sufficient to induce a reaction on the surface of the TiO_2 photocatalyst. During the excitation process, a positively charged vacancy or hole (h^+) can generate several active species, such as ·OH and $\cdot O_2$, to mineralize the pollutants in water. In addition, research has shown that the reaction rate increases linearly with increasing light intensity at relatively low light intensities (<25 $mW \cdot cm^{-2}$), but with the increase of light intensity, the incident photon-to-current efficiency decreased due to few delivered photons being converted into electrons and transported through the external electrical circuit (Herrmann 1999; Garcia-Segura *et al.* 2018). Clearly, even though the UV intensity produced in the discharge is small (Zhang *et al.* 2013a), it can activate the TiO_2 catalyst. Therefore, a nanosized TiO_2 photocatalyst driven by discharge plasma is recognized as a potential technology, which has been applied to treat multifarious water contaminants. It is characterized by high energy utilization, excessive demineralization and less byproducts (Zhang *et al.* 2013b; Zhang *et al.* 2019). The main reaction mechanisms of the plasma catalyst system are shown as follows (Qin *et al.* 2009; He *et al.* 2014; Chang & Hu 2020):

$$TiO_2 \xrightarrow{plasma} e^- + h^+ \quad (1)$$

$$H_2O \xrightarrow{h^+} \cdot OH + H^+ \quad (2)$$

$$H_2O \xrightarrow{e^-} \cdot OH + H^+ \quad (3)$$

$$O_2 \xrightarrow{e^-} \cdot O_2^- \quad (4)$$

$$\cdot O + O_2 \longrightarrow O_3 + e^- \quad (5)$$

$$e^- + O_2 \longrightarrow \cdot HO_2 \quad (6)$$

$$2 \cdot HO_2 \longrightarrow O_2 + H_2O_2 \quad (7)$$

$$\cdot OH + \cdot OH \longrightarrow H_2O_2 \quad (8)$$

$$O_3 \xrightarrow{e^-} \cdot O + O_2 + e^- \quad (9)$$

In our previous work, multi-walled carbon nanotubes (MWCNTs) embedded with TiO_2 supported on γ-Al_2O_3 pellet (TiO_2-MWCNTs/γ-Al_2O_3) composite photocatalysts were used to remove azo dye in a discharge plasma system

(Li *et al.* 2016). Although we obtained a high removal rate of azo dye after 60 min treatment, the TiO_2 still suffers from some drawbacks, such as low quantum efficiency, high recombination rate, large band gap (3.2 eV) and low activity (Hashimoto *et al.* 2005). Over the past decades, metal-doped TiO_2 photocatalysts have been widely studied for improved photocatalytic performance in the degradation of various organic pollutants. However, doping metal showed several disadvantages: thermal instability of doped TiO_2, electron trapping by the metal centers, and the requirement of more expensive ion-implantation facilities (Yamashita *et al.* 1998; Wang *et al.* 1999). Since a breakthrough work by Asahi *et al.* (2001) in 2001 reported that doping TiO_2 with N can enhance its photocatalytic activity for the degradation of methylene blue under visible light irradiation, there has been a fruitful research strategy to narrow the band gap of TiO_2 and extend the light response range towards the visible region by doping with non-metal and transition metals (Inturi *et al.* 2014; Giannakasa *et al.* 2016). Among these non-metals and transition metals, N and V are the most promising dopants because the 2p orbital of N is the easiest to bind with the 2p orbital of O in the TiO_2 lattice to form the O-Ti-N structure (Schneider *et al.* 2014), while V ionic radii are almost the same as that of Ti^{4+}; thus, V^{4+} ions would probably be easier to substitute Ti^{4+} ions in the crystal lattice of TiO_2 (Ren *et al.* 2015).

In this work, a V and N co-doping TiO_2-MWCNTs/γ-Al_2O_3 (V/N-TiO_2-MWCNTs/γ-Al_2O_3) composite catalyst was prepared to enhance the removal of acid orange II (AO7) in a pulsed discharge plasma system. The aim of the work is to investigate the synergistic effects of pulsed discharge plasma and the V/N-TiO_2-MWCNTs/γ-Al_2O_3 composite photocatalyst. A series of characterization techniques, such as XRD, FTIR, SEM, XPS, etc., were carried out to determine the structure and surface chemical states of as-prepared composite catalyst. The enhancement effects of the doped amount of V and N, electrical factors and solution conditions on AO7 removal were investigated. The repetitive use of composite photocatalyst under pulsed discharge plasma was evaluated. The removal mechanism of AO7 from aqueous solution was also analyzed for the pulsed discharge plasma system with the V/N-TiO_2-MWCNTs/γ-Al_2O_3 composite.

EXPERIMENTAL

Materials

The MWCNTs (diameter > 50 nm, purity > 95%, tube length 10–20 nm) were purchased from Chengdu Organic Chemistry Co., Ltd, China. Prior to use, the MWCNTs should be acidified with concentrated sulfuric acid and concentrated nitric acid, whose volume ratio was 3:1 as Liang *et al.* (2017) described. The temperature was maintained at 50 °C for 5 h and reflux condensation was conducted at the same time. The sphere γ-Al_2O_3 (diameter 1–3 mm) was supplied by Henan Sanyi Water Treatment Technology Co., Ltd, China. The AO7 (AR, $C_{16}H_{11}N_2NaO_4S$, molecular weight = 350.32 g·mol^{-1}, purity 99.7%) was obtained from Shanghai Aladdin Bio-Chem Technology Co., Ltd, China. The silane coupling agent KH550 ($C_9H_{23}NO_3Si$) was received from Jinan Xingfei Long Chemical Co., Ltd, China. The ammonium metavanadate (AR, NH_4VO_3, molecular weight = 116.98 g·mol^{-1}) was purchased from Shanghai Shanpu Chemical Reagent Co., Ltd, China. The diethylamine (AR, $(C_2H_5)_2NH$) was received from Tianjin Tianli Chemical Reagent Co., Ltd, China. All other reagents used in this study, including titanium butoxide, acetyl acetone, absolute alcohol, nitric acid, glacial acetic acid, etc., were all AR grade and were obtained from Tianjin Kermel Chemical Reagent Co., Ltd, China.

Preparation and characterization of photocatalysts

The TiO_2-MWCNTs/γ-Al_2O_3 composite was prepared according to our previous work (Li *et al.* 2016). The details of synthetic procedures of the V/N-TiO_2-MWCNTs/γ-Al_2O_3 composite catalyst were described in the Supplementary Material. A series of V/N-TiO_2-MWCNTs/γ-Al_2O_3 composites were prepared by changing the concentration of NH_4VO_3 and $(C_2H_5)_2NH$, and they are denoted as V_x/N_y-TiO_2-MWCNTs/γ-Al_2O_3, where x and y represented the molar amounts of V and N in the composite, respectively.

The prepared photocatalysts were characterized by a range of analytical techniques. The crystal structures of the prepared photocatalysts were measured by X-ray diffractometry (XRD, Bruker D8 Advance A25, Germany) in the range of 20–80° using Cu Kα radiation. Fourier transform infrared spectroscopy (FTIR, Optics Tensor 27, USA) was used to analyze the composition information and chemical bonds of the samples. The surface morphologies of the photocatalysts were observed by a field emission scanning electron microscopy (FESEM, Hitachi S-4800, Japan). The surface chemical compositions of the photocatalysts were determined by X-ray photoelectron spectroscopy (XPS, EscaLab 250Xi, USA). UV-Vis diffuse reflectance spectroscopy of the samples was measured by a scanning UV-Vis spectrophotometer (UV-2600, Shimadzu, Japan) in the range of 300–800 nm. Photocurrent measurements were

carried out under visible light irradiation using a high-pressure xenon lamp.

Experimental procedures

The experimental device diagram has been described in our previous paper (Li *et al.* 2016). In each batch experiment, 300 mL AO7 aqueous solution is treated, and the initial concentration of AO7 is 50 mg·L^{-1}. The 5.0 g catalysts are filled between a high voltage multi-needle electrode and ground plate electrode. Prior to discharge treatment, air continuously bubbled into the reactor with a flow rate of 6.5 L·min^{-1}. The flow rate of the wastewater was 100 L·min^{-1}. The pulsed peak voltage and pulsed frequency used in the study is 22.8 kV and 75 Hz unchanged, respectively, unless special illustration.

A UV-Vis spectrophotometer was used as the analytical technique for monitoring the concentration reduction of the AO7 during the experiment because of its simplicity of use and ability to measure concentrations within a short time. A total organic carbon analyzer (TOC-L CPH, Shimadzu, Japan) was employed to determine the residual amounts of organic substances in the effluent to investigate the mineralization degree of the AO7 solution. The AO7 samples were drawn from the solution at 10 min intervals and analyzed using a UV-Vis spectrophotometer at 486 nm. A calibration curve is prepared from which the removal rate (η) of AO7 is calculated using Equation (10):

$$\eta = \frac{C_0 - C_t}{C_0} \times 100\% \tag{10}$$

The energy density (ED, g·kW^{-1}·h^{-1}) of the reactor is defined as the quantity of removed AO7 (g) per discharge power (kW·h) during treatment, as calculated by Equation (11):

$$ED = \frac{C_0 \times V \times \frac{C_0 - C_t}{C_0} \times \frac{1}{1000}}{\int_0^T UIdt} \tag{11}$$

where C_0 is the initial concentration of AO7 (mg·L^{-1}), and C_t is the concentration of AO7 after t min of treatment (mg·L^{-1}); T (h) is the treatment time and U and I are discharge voltage (kV) and current (A), respectively; V (mL) is the solution volume.

RESULTS AND DISCUSSION

Characterization of the composite catalysts

The as-prepared samples were characterized by XRD and FTIR. As seen from Figure 1(a), all diffraction peaks from the TiO_2-MWCNTs and V/N-TiO_2-MWCNTs composites are attributable to anatase TiO_2, which are consistent with the values in the standard card. No characteristic peaks attributed to V or N oxides are detected, indicating that the V and N ions were successfully incorporated into the crystal lattice of anatase TiO_2. The (101) peak intensity of TiO_2-MWCNTs decreases after V and N co-doping due to the formation of V-O-Ti or N-Ti-O linkages, which hinders the crystal growth as well as the agglomeration of TiO_2 particles (Chen *et al.* 2017a). It is also noticed that for the (101) plane peak, a small shift toward a lower diffraction angle occur in the peak position only for the V/N-TiO_2-MWCNTs composite sample, suggesting that the majority

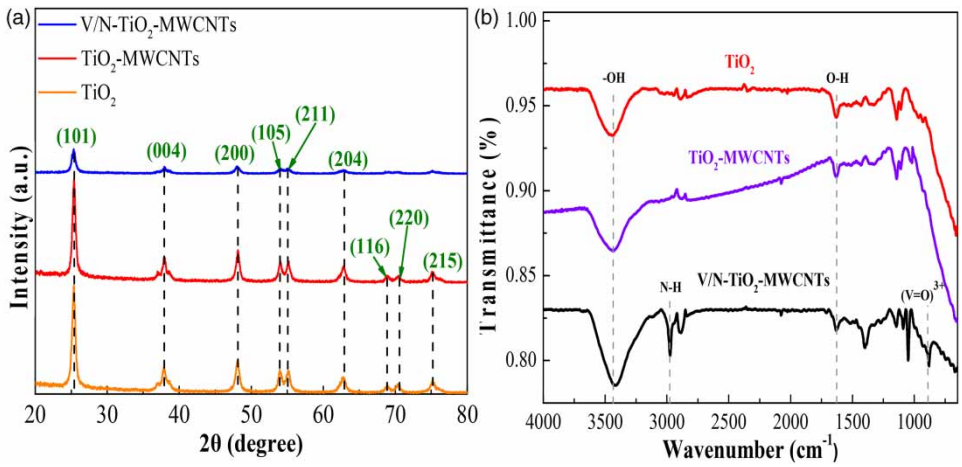

Figure 1 | XRD (a) and FTIR (b) spectra of prepared TiO_2, TiO_2-MWCNTs and V/N-TiO_2-MWCNTs composites.

of V and N ions might be successfully incorporated into the crystal lattice of anatase TiO_2 as V^{4+} or N^{4+} groups, and substituted for Ti and O in the crystal lattice of TiO_2 (Zhong *et al.* 2014).

Figure 1(b) shows the compositional information and chemical bonds of TiO_2, TiO_2-MWCNTs and V/N-TiO_2-MWCNTs composites analyzed by FTIR spectroscopy. The band at approximately 400–700 cm^{-1} represents a characteristic absorption peak of the Ti-O-Ti stretching vibration. The spectrum of the V/N-TiO_2-MWCNTs composite shows that near 860 cm^{-1} represents a characteristic stretching vibration peak of the $(V=O)^{3+}$ (Frederickson & Hausen 1963). The peak at 1,180 cm^{-1} is related to the C-O stretching vibration band of MWCNTs, which may result from the strong interaction between TiO_2-MWCNTs nanoparticles (Sangari *et al.* 2015). The band at approximately 3,000 cm^{-1} represents a characteristic absorption peak of the N-H stretching vibration, which may improve the activity of the catalyst due to the formation of intermolecular hydrogen bonds between the amide bonds. The presence of -OH groups and water on the surface of the particles is confirmed by the appearance of a broad band near 3,400 cm^{-1} for all samples. Another peak associated with O-H bending appeared at approximately 1,640 cm^{-1} (Kuvarega *et al.* 2012). Given that most characteristic peaks of MWCNTs, TiO_2, V and N are observed, the existence of MWCNTs, TiO_2, V and N in V/N-TiO_2-MWCNTs composite can be further confirmed.

Figure 2 shows the SEM images of the TiO_2, TiO_2-MWCNTs and V/N-TiO_2-MWCNTs composite. It can be seen from Figure 2(a) that the synthesized TiO_2 nanoparticles possess a near spherical shape and some of them reunite. From Figure 2(b), the TiO_2 nanoparticles appear to be homogenously deposited on the MWCNTs, but show

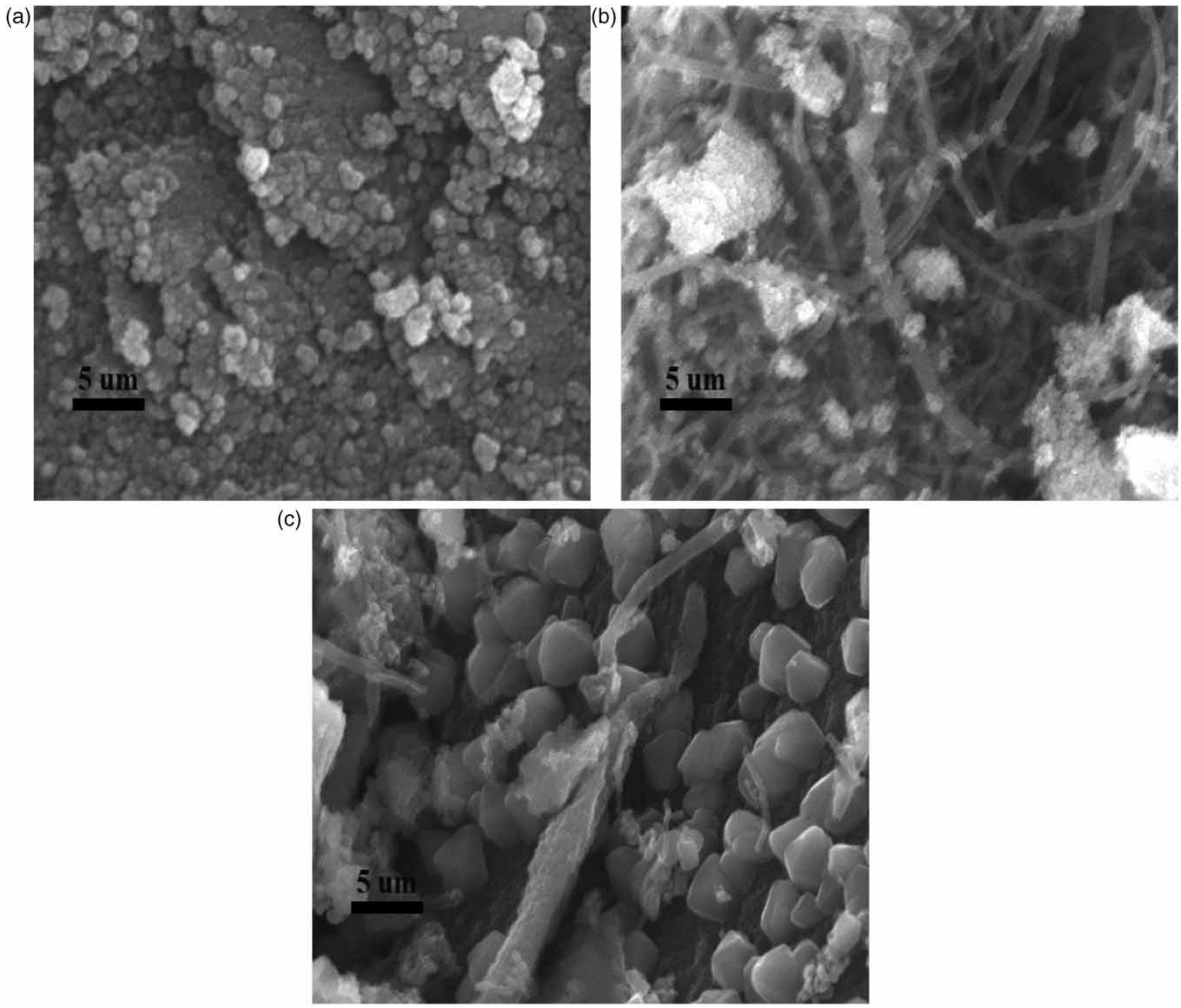

Figure 2 | SEM images of prepared catalysts: TiO_2 (a), TiO_2-MWCNTs composite (b), V/N-TiO_2-MWCNTs composite (c).

some agglomeration along the MWCNTs (Yan *et al.* 2006; Abd Hamid *et al.* 2014). The aggregation of TiO_2 over $MWCNT_S$ indicates the supporting role of $MWCNT_S$ as inhibiting the growth of TiO_2. As shown in Figure 2(c), the V, N and TiO_2 nanoparticles are well attached to the MWCNTs. Compared with Figure 2(b), many small particles are observed, which represent that V and N elements are doped on the surface of TiO_2. It is clear that V, N and TiO_2 nanoparticles are closely integrated and gathered on the MWCNTs, which is due to the high viscosity of the solid, thus reducing the dispersion of the particles. It is consistent with the XRD analysis that the structure of TiO_2 does not change after the loading of MWCNTs, V and N.

To further study the surface chemical composition and chemical state, the V/N-TiO_2-MWCNTs composite was characterized by XPS. As shown in Figure 3(a), the signals of C, Ti, O, V and N are detected in the survey XPS spectrum of the V/N-TiO_2-MWCNTs composite. No peaks of other elements are found, which means that the V/N-TiO_2-MWCNTs composite heterojunction photocatalyst is mainly composed of C, Ti, O, V and N elements. The XPS signals of Ti 2p are observed at binding energies at approximately 457.6 eV (Ti $2p_{3/2}$) and 463.3 eV (Ti $2p_{1/2}$), as shown in Figure 3(b), which is the binding energy consistent with Ti^{4+} oxidation state (Wang *et al.* 2015). The O 1s high resolution spectra of V/N-TiO_2-MWCNTs composite are fitted to two peaks in Figure 3(c). The peak at approximately 530 eV corresponds to the Ti-O bond (Cong *et al.* 2011), which means that the chemical state of oxygen is the main lattice oxygen in TiO_2. The peaks at 531.5 eV are assigned to the O-H bond. Figure 3(d) displays the high-resolution peak fitting spectra of N 1s. The four peaks at 398.3 eV, 398.7 eV, 399.1 eV and 400.2 eV correspond to sp^2 hybridized nitrogen (C-N-C), N-Ti-N, tertiary nitrogen (N-$(C)_3$) and N-H, respectively (Li *et al.* 2005; Chen *et al.* 2014), which means that N elements are closely combined with MWCNTs and TiO_2 by forming new chemical bonds. Figure 3(e) shows the C 1s spectrum of V/N-TiO_2-MWCNTs composite with one C 1s peak at 283.7 eV, which is attributed to a C-C bond from MWCNTs (Li *et al.* 2005). As shown in Figure 3(f), the V 2p spectra of the V/N-TiO_2-MWCNTs composite have peaks at 516.9 eV (V $2p_{3/2}$) and 529.6 eV (V $2p_{1/2}$). The absorption peak at 516.9 eV is mainly due to V^{5+} $2p_{3/2}$ and V^{4+} $2p_{3/2}$. Since the doped amount of V is very small, the peak shape is weak, and the 529.6 eV may be the corresponding absorption peak of V^{4+} $2p_{3/2}$. The fitting data demonstrate that V^{4+} is the dominant composition on the surface of doped V/N-TiO_2-MWCNTs composite, which suggests that the ionic radius of V^{4+} is very close to that of Ti^{4+}, and V^{4+} can easily substituted for the Ti^{4+} into the TiO_2 crystal lattice (Patel *et al.* 2014; Ren *et al.* 2015).

Removal performance of AO7

Comparison of the removal performance

The photocatalytic activity of the blank without catalyst (namely, plasma alone), γ-Al_2O_3, TiO_2/γ-Al_2O_3, TiO_2-MWCNTs/γ-Al_2O_3 and V/N-TiO_2-MWCNTs/γ-Al_2O_3 composites in the removal of AO7 were compared in the pulsed discharge plasma system, respectively, and the results are shown in Figure 4. Figure 4(a) shows that plasma coupled with the V/N-TiO_2-MWCNTs/γ-Al_2O_3 composite shows better photocatalytic activity in the removal of AO7 compared to plasma coupled with TiO_2-MWCNTs/γ-Al_2O_3 composite, TiO_2/γ-Al_2O_3 composite and γ-Al_2O_3 as well as plasma alone. Under the pulsed discharge plasma, 81.3% AO7 is removed by the TiO_2-MWCNTs/γ-Al_2O_3 composite after 10 min. The removal rate of AO7 increases to 100% after 10 min by the V/N-TiO_2-MWCNTs/γ-Al_2O_3 composite. This may be due to the V and N co-doping causing TiO_2 lattice distortion and introducing a new impurity energy level in the band gap with V and N co-doping, which not only reduces the band gap of TiO_2 but also inhibits the recombination of the e^-/h^+ pairs. Therefore, the synergistic effects of V and N enhance the photocatalytic activity of TiO_2 (Zhang *et al.* 2014). To gain an insight into the rate of different reaction systems, the kinetic model was also implemented to describe the removal rate. The reaction kinetics of AO7 for different treatment systems are shown in Figure 4(b) and the reaction rate constants are listed in Table 1. It is observed from Figure 4(b) that under pulsed discharge plasma, the removal rate of TiO_2/γ-Al_2O_3, γ-Al_2O_3 and plasma alone to AO7 follow the pseudo first-order, as verified by $\ln(C_t/C_0) = kt$. The removal rate of plasma coupled with the TiO_2-MWCNTs/γ-Al_2O_3 and V/N-TiO_2-MWCNTs/γ-Al_2O_3 composites to AO7 follow the pseudo second order kinetics model ($t/q_t = 1/(kq_e^2) + t/q_e$). The V/N-$TiO_2$-MWCNTs/$\gamma$-$Al_2O_3$ composite exhibits excellent photocatalytic activity, and the rate constant k ($k = 1.0496\ g{\cdot}mg^{-1}{\cdot}min^{-1}$) of the reaction is 5.99 and 72.39 times that of TiO_2-MWCNTs/γ-Al_2O_3 ($k = 0.1752\ g{\cdot}mg^{-1}{\cdot}min^{-1}$) and TiO_2/γ-Al_2O_3 ($k = 0.0145\ g{\cdot}mg^{-1}{\cdot}min^{-1}$), respectively. It is further confirmed that MWCNTs and V/N-TiO_2 connected by a heterojunction can significantly improve the photocatalytic reaction rate.

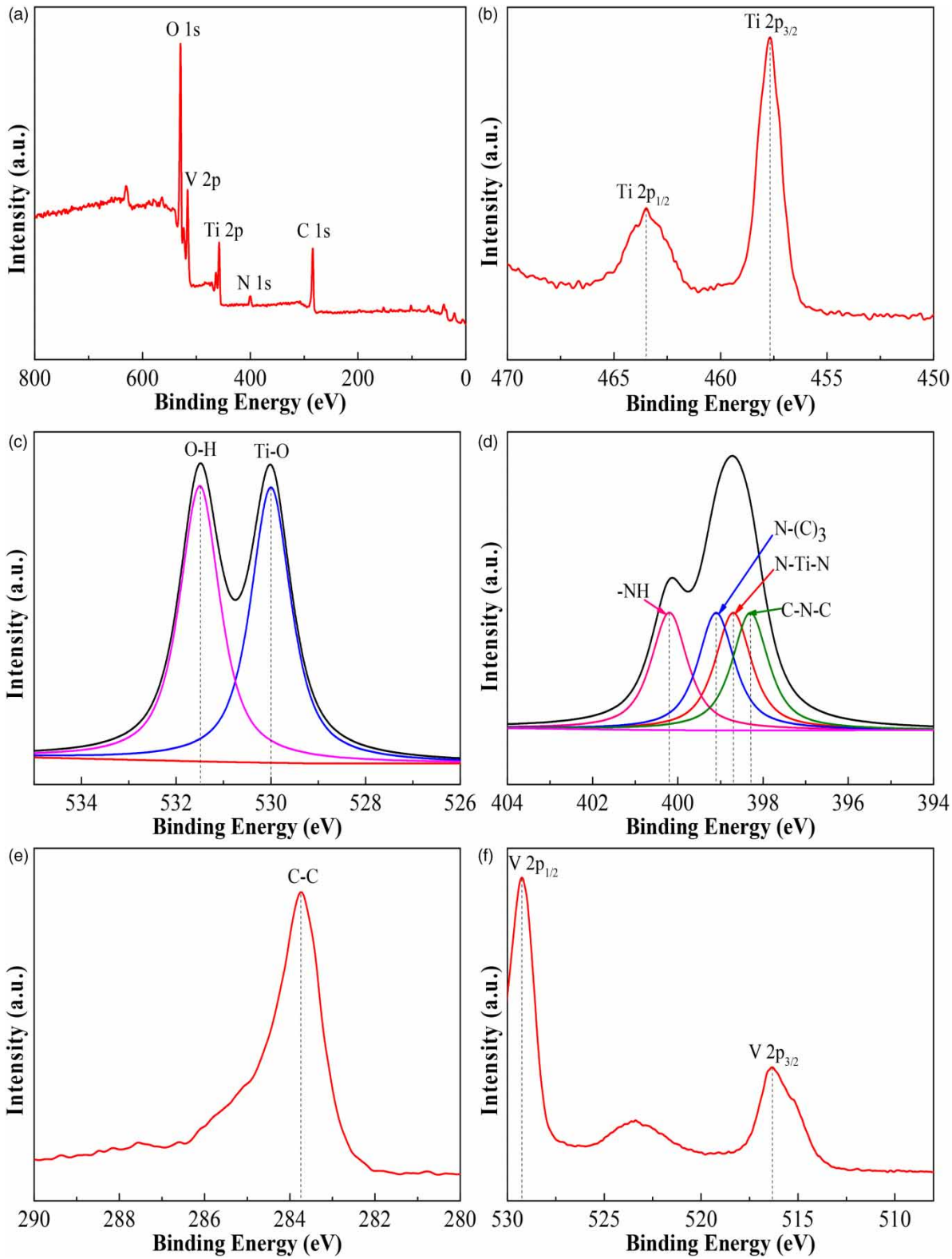

Figure 3 | XPS fully scanned spectra of V/N-TiO_2-MWCNTs composite (a), XPS spectra of Ti 2p (b), XPS spectra of O 1s (c), XPS spectra of N 1s (d), XPS spectra of C 1s (e) and XPS spectra of V 2p (f).

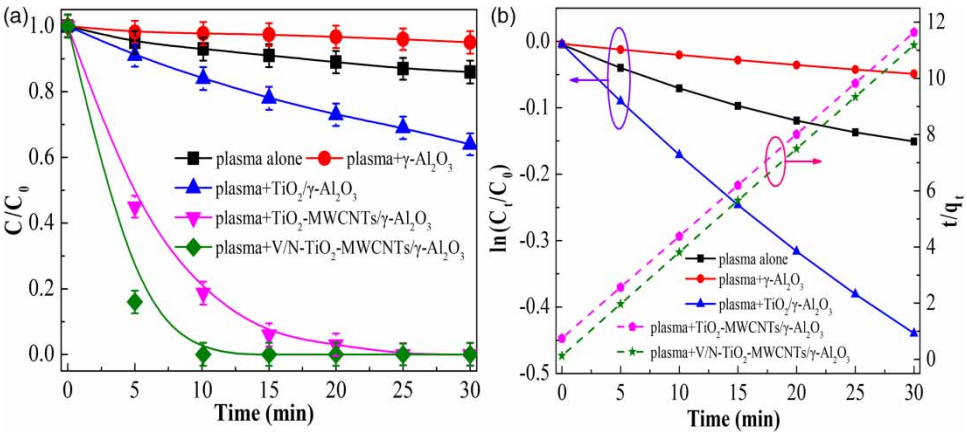

Figure 4 | Removal efficiencies and reaction kinetics of AO7 in different treatment systems.

Table 1 | Kinetic parameters of AO7 removal in different reaction systems

System	Response model	k	R^2
Plasma alone	$\ln(C_t/C_0) = kt$	$k = 0.0049$	0.9830
Plasma + γ-Al_2O_3		$k = 0.0015$	0.9603
Plasma + TiO_2/γ-Al_2O_3		$k = 0.0145$	0.9946
Plasma + TiO_2-MWCNTs/γ-Al_2O_3	$t/q_t = 1/(kq_e^2) + t/q_e$	$k = 0.1752$	0.9844
Plasma + V/N-TiO_2-MWCNTs/γ-Al_2O_3		$k = 1.0496$	0.9990

Note: k is reaction rate constant; R^2 is the rate equation fitting coefficient.

The effects of the doped amount of V and N in composite on AO7 removal

The effects of the doped amount of V and N in the V/N-TiO_2-MWCNTs/γ-Al_2O_3 composite on AO7 removal in pulsed discharge plasma system are shown in Figure 5. As observed in Figure 5, the $V_{0.10}/N_{0.05}$-TiO_2-MWCNTs/γ-Al_2O_3 composite exhibits the highest removal rate of 100% for AO7 under pulsed discharge plasma within 10 min. When n(V) = 0.1 mol, the removal tate of AO7 increases at first and then decreases with the increase of the amount of N. As the amount of V increases, the removal rate of AO7 increased initially and then decreased when n(N) = 0.05 mol. This may be due to overloaded co-doping of V and N in the V/N-TiO_2-MWCNTs/γ-Al_2O_3 composite that may result in channel plugging, and thus reduced photocatalytic activity of TiO_2. With the decrease of V and N co-doping, the recombination opportunity of e_{cb}^-/h_{vb}^+ pairs is reduced, which improves the photocatalytic activity of the catalyst. With the further reduction of V and N content in the V/N-TiO_2-MWCNTs/γ-Al_2O_3 composite, the photocatalytic activity of

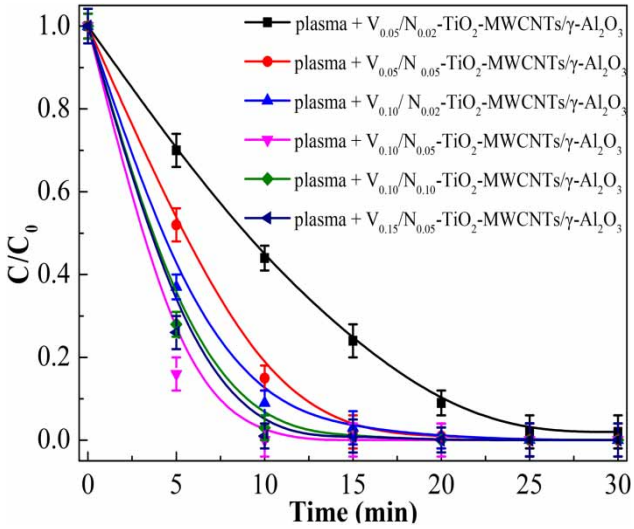

Figure 5 | Effects of doped ratio of V and N in the composite on AO7 removal for pulsed discharge plasma system.

TiO_2 decreases because it does not cause TiO_2 lattice distortion. It is an indication that the introduction of appropriate amounts of V and N ions into the TiO_2 lattice might effectively restrain the recombination rate of photogenerated e_{cb}^-/h_{vb}^+ pairs, resulting in enhancing the photocatalytic activity of TiO_2. Thus, $V_{0.10}/N_{0.05}$-TiO_2-MWCNTs/γ-Al_2O_3 composite was used in this study.

Effects of different electrical factors and solution conditions on AO7 removal

Figure 6(a) illustrates the effects of pulsed peak voltage on AO7 removal in a pulsed discharge plasma induced V/N-TiO_2-MWCNTs/γ-Al_2O_3 composite system. As shown in Figure 6(a), the removal rate of AO7 is enhanced with

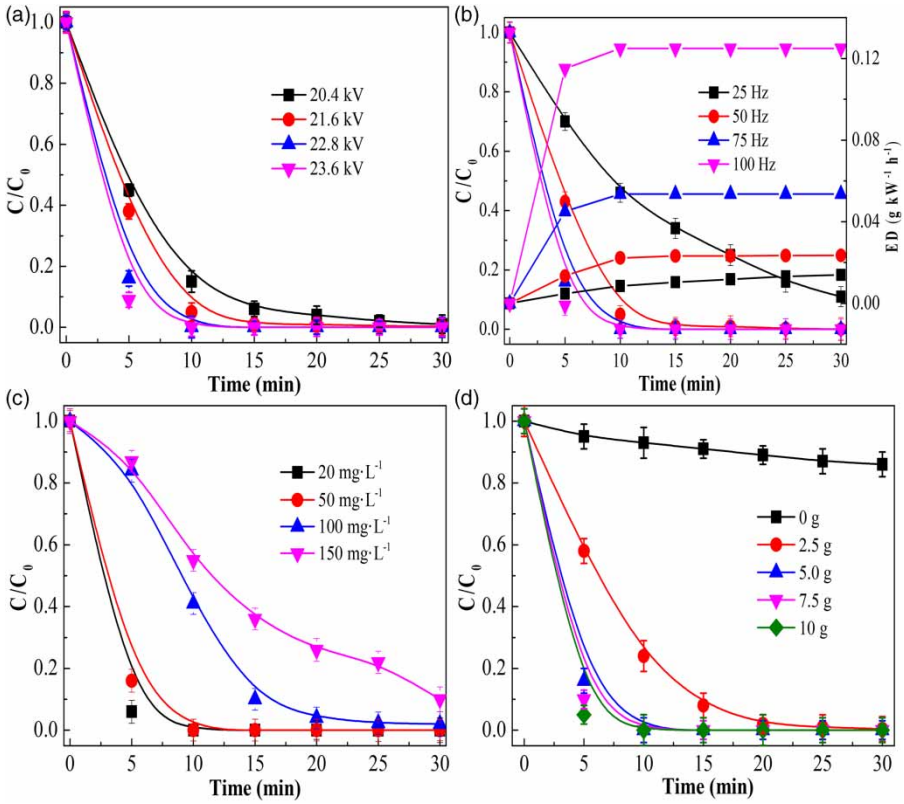

Figure 6 | Effects of pulsed peak voltage (a), pulsed frequency (b), initial concentration (c) and quantity of catalyst (d) on AO7 removal.

increasing pulsed peak voltage. At 20.4 kV, 85.0% of AO7 is removed after 10 min. The removal rate of AO7 increases to 100.0% after 10 min at 23.6 kV. With pulsed peak voltage increases, the electric field intensity is enhanced, and more active species are produced, such as O_3, •O, and •OH. In addition, with the voltage raised, the intensity of UV light and shockwave are also enhanced (Zhang *et al.* 2010; Chen *et al.* 2017b). This stronger irradiation can promote the formation of photogenerated e_{cb}^- and h_{vb}^+ in the V/N-TiO_2-MWCNTs/γ-Al_2O_3 composite. The photogenerated e_{cb}^- and h_{vb}^+ effectively promote the removal of AO7. Furthermore, the e_{cb}^- and h_{vb}^+ facilitate the generation of reactive species, such as •OH and $\bullet O_2^-$, on the catalyst when the V/N-TiO_2-MWCNTs/γ-Al_2O_3 composite' surface is irradiated (Tang *et al.* 2013). Figure 6(b) presents the effects of pulsed frequency on AO7 removal in the pulsed discharge plasma induced V/N-TiO_2-MWCNTs/γ-Al_2O_3 composite system. After 10 min of discharge treatment, the removal rate of AO7 is 54.0%, 95.0%, 100.0% and 100.0% with pulsed frequencies of 25 Hz, 50, 75 and 100 Hz under a pulsed peak voltage of 22.8 kV, respectively. It is obvious that the removal rate of AO7 is promoted with pulsed frequency increases. This can be explained by more energy being injected into the reactor per unit time at higher pulse repetitive frequency, resulting in a higher energy density per unit volume of the reactor (see Figure 6(b)). More micro-discharges are produced during each unit of time and the amount of high energetic electrons increases. These high energy electrons and generated species not only lead to more collision probabilities with AO7 in solution but also induce the V/N-TiO_2-MWCNTs/γ-Al_2O_3 composite to remove AO7 in solution (Snyder & Anderson 2001). Thus, the removal rate of AO7 is improved. Figure 6(c) displays the effects of the initial concentration on AO7 removal in the pulsed discharge plasma induced V/N-TiO_2-MWCNTs/γ-Al_2O_3 composite system. It can be seen from Figure 6(c) that the removal rate of AO7 decreases as the initial concentration of AO7 increases. At the initial concentration of 50.0 mg·L^{-1}, 100.0% of AO7 is removed within 10 min. When the initial concentration of AO7 reaches 150.0 mg·L^{-1}, the removal rate decreases to 45.0%. With the increasing AO7 concentration, more organic substances (AO7 and intermediates) are adsorbed on the surface of the V/N-TiO_2-MWCNTs/γ-Al_2O_3 catalysts, and the generation of active species, such as ·OH, ·O, H_2O_2 and O_3 is restrained. Additionally, adsorbed AO7 dye molecules at

high dye concentrations might block the active areas on the surface of the V/N-TiO_2-MWCNTs/γ-Al_2O_3 composite, causing minimal development of •OH radicals, which in turn results in the lower removal rate of AO7. Figure 6(d) depicts the effects of the quality of V/N-TiO_2-MWCNTs/γ-Al_2O_3 composite on the removal rate of AO7 in the pulsed discharge plasma system. The removal rate of AO7 distinctly increases when the amount of V/N-TiO_2-MWCNTs/γ-Al_2O_3 composite increases from 0 to 5.0 g. When the catalyst amount is 5.0 g, the removal rate of AO7 can reach 100.0% after 10 min of treatment in a pulsed discharge plasma system. A catalyst increase from 5.0 to 10.0 g in the amount exhibits a slow increase. These suggest that at lower levels of catalyst content, increasing the amount of catalyst provides more total surface area and active sites for both adsorption and photocatalysis, resulting in the enhancement of the removal rate. However, a further increase in the catalyst amount may cause light scattering and a screening effect affecting the specific activity of the catalyst (An *et al.* 2014). Additionally, it is important to keep the cost of the treatment low if it is to be industrially utilized; therefore, the optimum catalyst amount appears to be 5.0 g in this study.

Recycling experiments

The repetitive use of the composite is very important for its practical application. Hence, the stability of the V/N-TiO_2-MWCNTs/γ-Al_2O_3 composite was evaluated by reusing the catalyst 6 times for the removal of AO7. After each use, the catalyst was washed with ethanol, then acetone, and then dried in an oven at 60 °C for 1 h. As shown in Figure 7, the catalyst displays sufficient stability and reaches a maximum removal rate of 85.0% after 6 cycles under pulsed discharge plasma. We must admit that the catalyst had a loss after six experiments but the remaining 85% proved its potential catalytic performance and its value for practical application.

Mechanism of enhanced composite photocatalysis induced by pulsed discharge plasma

Figure 8 shows the UV-Vis DRS spectroscopy of TiO_2, TiO_2-MWCNTs and $V_{0.10}/N_{0.05}$-TiO_2-MWCNTs composites. As shown in Figure 8(a), the spectra are characterized by an intense fundamental absorption due to anatase TiO_2 in the region of between 350 and 400 nm. Meanwhile, the absorption edge of the TiO_2-MWCNTs and $V_{0.10}/N_{0.05}$-TiO_2-MWCNTs composites exhibits a dramatic red shift when

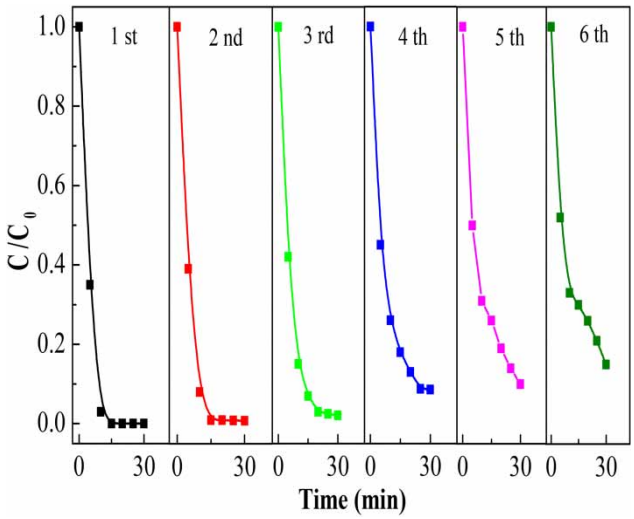

Figure 7 | Recyclability studies of the V/N-TiO_2-MWCNTs composite for AO7 removal in pulsed discharge plasma system.

compared with that of the pure TiO_2, which, due to the presence of MWCNTs, V and N doping, results in decreasing the energy gap for electron transition. Although TiO_2-MWCNTs composite has better absorbency and absorption edge range than $V_{0.10}/N_{0.05}$-TiO_2-MWCNTs composite, there are many factors that affect the photocatalytic activity of the catalyst. Therefore, it is not correct to think that the better the visible light absorption, the higher the catalytic activity. The doping of V and N can produce an effective interfacial electron transfer, which is helpful to the separation of e^-_{cb}/h^+_{vb} pairs on V/N-TiO_2-MWCNTs and the catalytic active point of the composite.

As shown in Figure 8(b), the band gap energies of the direct transition semiconductors were estimated by plots of $(\alpha h\nu)^{1/2}$ vs photon energy on the basis of the following formula (Ilkhechi *et al.* 2016):

$$(\alpha h\nu)^{1/2} = A\ (h\ \nu - E_g) \tag{12}$$

where α, h, ν, A and E_g represent the absorption coefficient, Planck's constant, optical frequency, constant and band gap, respectively. It can be estimated from Figure 8(b) that the band gap energies of TiO_2 and TiO_2-MWCNTs are 2.76 eV and 2.50 eV, respectively. The band gap of $V_{0.10}/N_{0.05}$-TiO_2-MWCNTs composite is significantly reduced to approximately 1.70 eV. This is because V and N introduce impurity energy levels at the conduction band (CB) bottom and the valence band (VB) edge, and the increase of impurity energy series leads to a further decrease of the band gap. In addition, the increase of impurity energy level also greatly

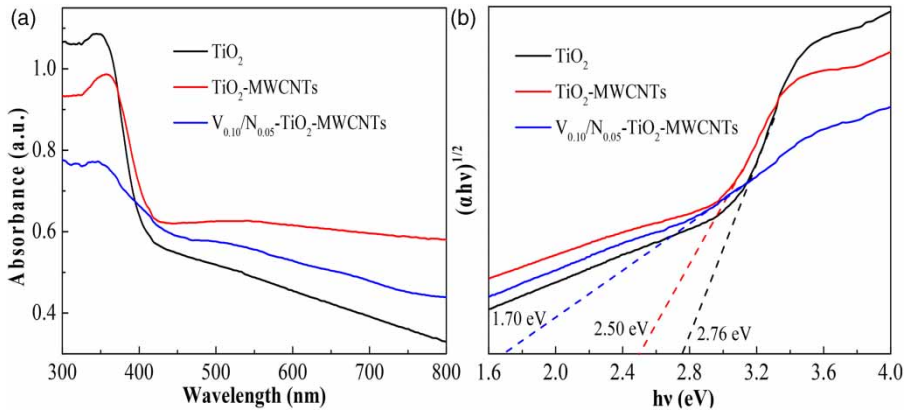

Figure 8 | UV-Vis spectra (a) and plots of $(\alpha h\nu)^{1/2}$ vs photon energy (b) of the prepared TiO_2, TiO_2-MWCNTs and $V_{0.10}/N_{0.05}$-TiO_2-MWCNTs composites.

reduces the VB electron's transition energy; that is, the VB electron can transfer to the CB with less energy absorption, and also promote the effective separation of photogenerated e^- and h^+, thereby enhancing the photocatalytic properties of TiO_2. This confirms that adding a small amount of N and V ion dopants could alter the absorption feature significantly.

Figure 9 shows the photocurrent response curves of the photoelectrodes consisting of TiO_2, TiO_2-MWCNTs and $V_{0.10}/N_{0.05}$-TiO_2-MWCNTs composites. It is found that the stable photocurrent values of TiO_2-MWCNTs and $V_{0.10}/N_{0.05}$-TiO_2-MWCNTs composites are nearly 2 and 4 times higher than that of pure TiO_2. It can be ascribed to V and N co-doping improving the separation rate of photogenerated e^- and h^+, and results in the enhancement of the photocurrent. The N anion and V cation co-doping TiO_2-MWCNTs can effectively reduce the complex center because co-doping avoids the defect band caused by single doping. The V and N co-doping catalyst has a better optical response capability, which is more advantageous to the generation and separation of photonic e^- and h^+.

Figure 10 displays the UV-Vis absorption spectra changes of AO7 solution degraded by $V_{0.10}/N_{0.05}$-TiO_2-MWCNTs composite induced by pulsed discharge plasma at different treatment times. It is found that AO7 has four absorption peaks at 235, 256, 310, and 486 nm and a shoulder peak at 425 nm. The peak at 486 nm suggests the presence of the hydrazone form (main adsorption peak), whereas the shoulder peak at 425 nm indicates the presence of the azo form. Under the given conditions, a rapid decoloration of the AO7 solution is fulfilled within 10 min. Moreover, with the disappearance of the characteristic peak at 486 nm, the intensities of the peaks at 235, 256

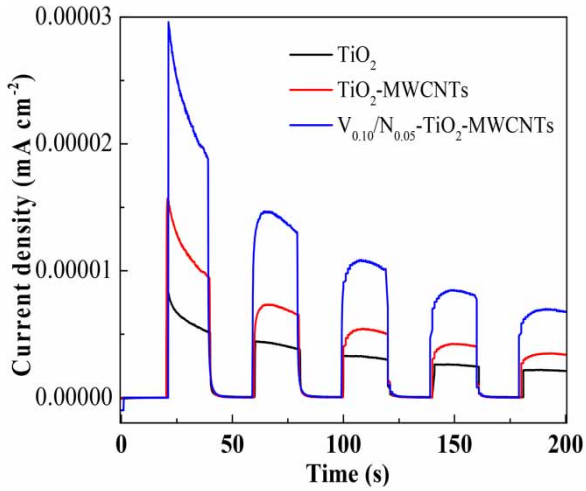

Figure 9 | The photocurrent response curves of the photoelectrodes consisting of TiO_2, TiO_2-MWCNTs and $V_{0.10}/N_{0.05}$-TiO_2-MWCNTs composites.

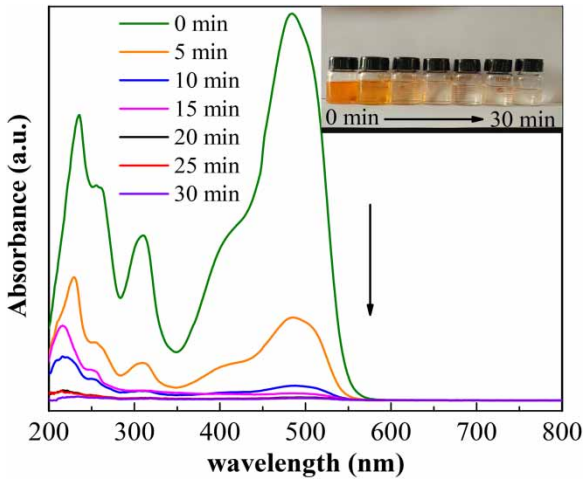

Figure 10 | The UV-Vis absorption spectra changes of AO7 solution at discharge plasma treatment times with $V_{0.10}/N_{0.05}$-TiO_2-MWCNTs composites.

and 310 nm are also decreased without the formation of new absorption peaks, which indicates that some structures are broken by the action of pulsed discharge plasma induced V/N-TiO_2-MWCNTs composite. In addition, it can also be inferred from Figure 10 that radicals generated during the reaction process reacted with the azo group (-*N*=N-) responsible for the characteristic color of the dye, whereas the radical reaction with the other four groups is weak. It may be due to the -*N*=N- in the AO7 molecule being unstable and prone to be attacked by the activated species. Thus, the generated radicals easily react with the -*N*=N- and make the group rupture during the oxidation reaction. Furthermore, no new peaks came into being both in the ultraviolet area and in the visible light area, which indicate the naphthyl and benzene ring, containing fragments generated during the decoloration process, were further degraded (Guo *et al.* 2016). As a good indicator of the mineralization of organic pollutants, the variation of TOC was monitored. As shown in Figure 11, the TOC removal is 50.2% for the pulsed discharge plasma induced $V_{0.10}/N_{0.05}$-TiO_2-MWCNTs composite system, which is 2.3 and 1.2 times higher than that in the pulsed discharge plasma system alone and pulsed discharge plasma induced TiO_2-MWCNTs composite system, respectively. The results confirm that the synergetic effects of pulsed discharge plasma and V/N-TiO_2-MWCNTs composite have good removal rates and certain mineralization of AO7 (Figure 12). The relatively low removal of TOC indicates that there is still a portion of the intermediate organics in the solution. The reason may be that AO7 molecules in solution are not directly mineralized into CO_2 and H_2O during the removal process. It is degraded into some intermediate products through degradation of chromophoric groups and benzene-like ring structure, and then degraded into CO_2 and H_2O.

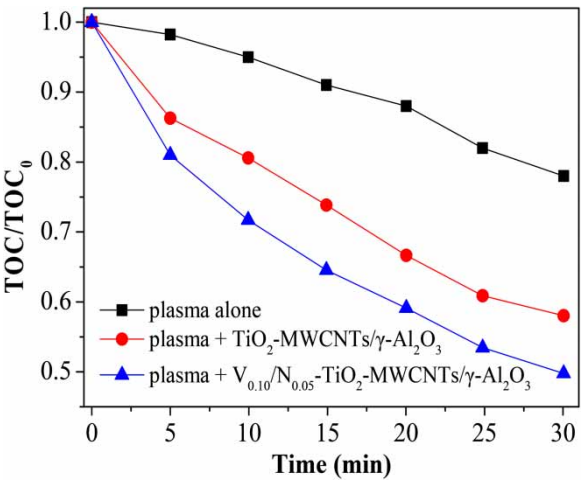

Figure 11 | The changes of TOC after different discharge plasma treatment times with $V_{0.10}/N_{0.05}$-TiO_2-MWCNTs composite.

CONCLUSIONS

The synergistic effects of the pulsed discharge plasma and V/N-TiO_2-MWCNTs/γ-Al_2O_3 composite photocatalyst significantly enhance the removal rate of the azo dye AO7 from aqueous solution. Under pulsed discharge plasma, almost 100% of AO7 is removed by the V/N-TiO_2-

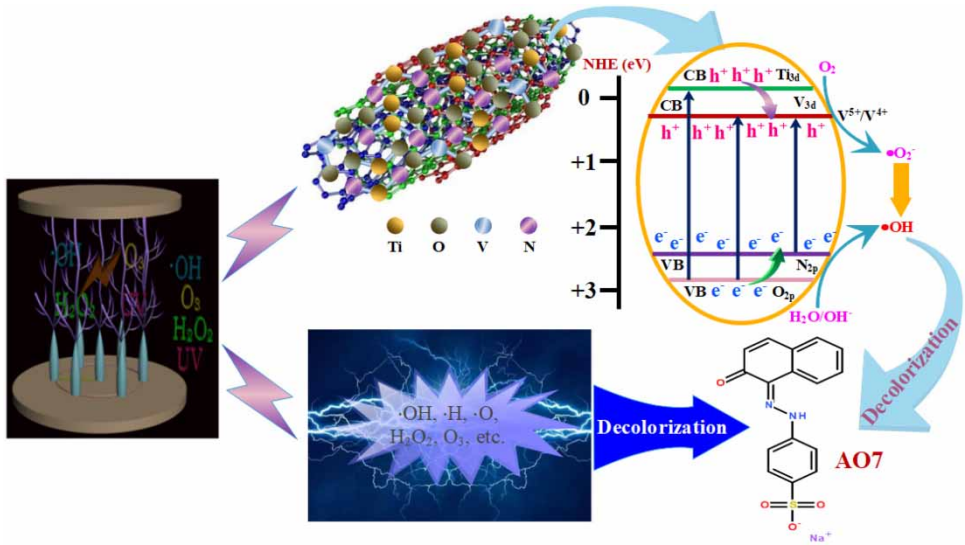

Figure 12 | The proposed mechanism of synergetic effect of pulsed discharge plasma and V/N-TiO_2-MWCNTs composite for AO7 removal from aqueous solution.

MWCNTs/γ-Al_2O_3 composite after 10 min under optimal conditions. Removal of AO7 can be significantly enhanced by the pulsed discharge plasma induced V/N-TiO_2-MWCNTs/γ-Al_2O_3 composite because V and N co-doping causes TiO_2 lattice distortion and introduces a new impurity energy level, which not only reduces the band gap of TiO_2 but also inhibits the recombination of the e^-_{cb}/h^+_{vb} pairs. The doping ratio V and N is important to enhance the activity of TiO_2 because overloaded doping of V and N may result in channel plugging. The removal rate of AO7 is also affected by the pulsed discharge peak voltage, pulsed discharge frequency, initial concentration of the solution and dosage of the composite catalyst. For application purposes, V/N-TiO_2-MWCNTs/γ-Al_2O_3 composite catalysts demonstrate an adequate recycling performance, proving it to be a viable option for degrading organic pollutants from aqueous solution in a pulsed discharge plasma system. Pulsed discharge plasma induced V/N-TiO_2-MWCNTs/γ-Al_2O_3 composite photocatalyst can effectively break down AO7, but cannot completely break AO7 down into CO_2 and H_2O.

ACKNOWLEDGEMENTS

The authors gratefully acknowledge the financial support provided by the National Natural Science Foundation of China (grant No. 21107085), the Overseas Student's Science and Technology Activities Project Merit Funding of Shaanxi and the Fundamental Research Funds for the Central Universities (grant No. 2452017106).

DATA AVAILABILITY STATEMENT

All relevant data are included in the paper or its Supplementary Information.

REFERENCES

Abd Hamid, S. B., Tan, T. L., Lai, C. W. & Samsudin, E. M. 2014 Multiwalled carbon nanotube/TiO_2 nanocomposite as a highly active photocatalyst for photodegradation of Reactive Black 5 dye. *Chin. J. Catal.* **35**, 2014–2019.

An, Y., Hou, J., Liu, Z. Y. & Peng, B. H. 2014 Enhanced solid-phase photocatalytic degradation of polyethylene by TiO_2-MWCNTs nanocomposites. *Mater. Chem. Phys.* **148**, 387–394.

Asahi, R., Morikawa, T., Ohwaki, T., Aoki, K. & Taga, Y. 2001 Visible-light photocatalysis in nitrogen-doped titanium oxides. *Science* **293**, 269–271.

Chang, C. W. & Hu, C. 2020 Graphene oxide-derived carbon-doped $SrTiO_3$ for highly efficient photocatalytic degradation of organic pollutants under visible light irradiation. *Chem. Eng. J.* **383**, 116–123.

Chen, Y. F., Huang, W. X., He, D. L., Yue, S. T. & Huang, H. 2014 Construction of heterostructured g-C_3N_4/Ag/TiO_2 microspheres with enhanced photocatalysis performance under visible-light irradiation. *ACS Appl. Mater. Interfaces* **6**, 14405–14414.

Chen, Y., Wu, Q., Zhou, C. & Jin, Q. T. 2017a Enhanced photocatalytic activity of La and N co-doped TiO_2/diatomite composite. *Powder Technol.* **322**, 296–300.

Chen, J. Y., Du, Y. L., Shen, Z. J., Lu, S. S., Su, K. Z., Yuan, S. J., Hu, Z. H., Zhang, A. Y. & Feng, J. W. 2017b Non-thermal plasma and $BiPO_4$ induced degradation of aqueous Crystal violet. *Sep. Purif. Technol.* **179**, 135–144.

Cong, Y., Li, X. K., Qin, Y., Dong, Z. J., Yuan, G. M., Cui, Z. W. & Lai, X. J. 2011 Carbon-doped TiO_2 coating on multiwalled carbon nanotubes with higher visible light photocatalytic activity. *Appl. Catal. B-Environ.* **107**, 128–134.

Frederickson, L. D. & Hausen, D. M. 1963 Infrared spectra-structure correlation study of vanadium-oxygen compounds. *Anal. Chem.* **35**, 1167–1167.

Fujishima, A., Rao, T. N. & Tryk, D. A. 2000 Titanium dioxide photocatalysis. *J. Photochem. Photobiol. C Photochem. Rev.* **1**, 1–21.

Garcia-Segura, S., O'Neal Tugaoen, H., Hristovski, K. & Westerhoff, P. 2018 Photon flux influence on photoelectrochemical water treatment. *Ele.Commu. J.* **87**, 63–65.

Giannakasa, A. E., Antonopouloua, M., Daikopoulos, C., Deligiannakis, Y. & Konstantinou, I. 2016 Characterization and catalytic performance of B-doped, B-N co-dopedand B-N-F tri-doped TiO_2 towards simultaneous Cr(VI) reduction and benzoic acid oxidation. *Appl. Catal. B-Environ.* **184**, 44–54.

Guo, H., Wang, H. J., Wu, Q. S., Zhou, G. S. & Yi, C. W. 2016 Kinetic analysis of acid orange 7 degradation by pulsed discharge plasma combined with activated carbon and the synergistic mechanism exploration. *Chemosphere* **159**, 221–227.

Hashimoto, K., Irie, H. & Fujishima, A. 2005 TiO_2 photocatalysis: a historical overview and future prospects. *Jpn. J. Appl. Phys.* **44**, 8269–8285.

He, D., Sun, Y. B., Xin, L. & Feng, J. W. 2014 Aqueous tetracycline degradation by non-thermal plasma combined with nano-TiO_2. *Chem. Eng. J.* **258**, 18–25.

Herrmann, J. M. 1999 Heterogeneous photocatalysis: fundamentals and applications to the removal of various types of aqueous pollutants. *Catal. Today* **53**, 115–129.

Ilkhechi, N. N., Azar, Z., Khajeh, M. & Mozamme, M. 2016 Enhanced structural, optical and super-hydrophilic properties of TiO_2 thin film co-doped by V and Sn. *J. Mater. Sci. Mater. El* **27**, 10541–10549.

Inturi, S. N. R., Boningari, T., Suidan, M. & Smirniotis, P. G. 2014 Visible-light-induced photodegradation of gas phase

acetonitrile using aerosol-made transition metal (V, Cr, Fe, Co, Mn, Mo, Ni, Cu, Y,Ce, and Zr) doped TiO_2. *Appl. Catal. B-Environ.* **144**, 333–342.

Jiang, B., Zheng, J. T., Liu, Q. & Wu, M. B. 2012 Degradation of azo dye using nonthermal plasma advanced oxidation process in a circulatory airtight reactor system. *Chem. Eng. J.* **204**, 32–39.

Jiang, B., Zheng, J. T., Qiu, S., Wu, M. B., Zhang, Q. H., Yan, Z. F. & Xue, Q. Z. 2014 Review on electrical discharge plasma technology for wastewater remediation. *Chem. Eng. J.* **236**, 348–368.

Joshi, A. A., Locke, B. R., Arce, P. & Finney, W. C. 1995 Formation of hydroxyl radicals, hydrogen-peroxide and aqueous electrons by pulsed streamer corona discharge in aqueous-solution. *J. Hazard. Mater.* **41**, 3–30.

Kuvarega, A. T., Krause, R. W. M. & Mamba, B. B. 2012 Multiwalled carbon nanotubes decorated with nitrogen, palladium co-doped TiO_2 (MWCNT/N, Pd co-doped TiO_2) for visible light photocatalytic degradation of Eosin Yellow in water. *J. Nanopart. Res.* **14**, 776–792.

Li, H., Hao, Y. B., Lu, H. Q., Liang, L. P., Wang, Y. Y., Qiu, J. H., Shi, X. C., Wang, Y. & Yao, J. F. 2005 A systematic study on visible-light N-doped TiO_2 photocatalyst obtained from ethylenediamine by sol-gel method. *Appl. Surf. Sci.* **344**, 112–118.

Li, X., Wang, T. C., Qu, G. Z., Liang, D. L. & Hu, S. B. 2016 Enhanced degradation of azo dye in wastewater by pulsed discharge plasma coupled with MWCNTs-TiO_2/γ-Al_2O_3 composite photocatalyst. *J. Environ. Manage.* **172**, 186–192.

Liang, J. C., Zhang, X. L., Yu, K. F. & Liang, C. 2017 TiO_2 hollow nanocrystals/carbon nanotubes nanocomposite and their application in lithium-ion batteries. *ChemistrySelect* **2**, 4912–4919.

Locke, B. R., Sato, M., Sunka, P., Hoffmann, M. R. & Chang, J. S. 2006 Electrohydraulic discharge and nonthermal plasma for water treatment. *Ind. Eng. Chem. Res.* **45**, 882–905.

Murthy, M., Tubaki, S., Lokesh, S. V. & Rangappa, D. 2017 Co, N-doped TiO_2 coated r-GO as a photo catalyst for enhanced photo catalytic activity. *Mater. Today Proc.* **4**, 11873–11881.

Patel, N., Jaiswal, R., Warang, T., Scarduelli, G., Dashora, A., Ahuja, B. L., Kothari, D. C. & Miotello, A. 2014 Efficient photocatalytic degradation of organic water pollutants using V-N-codoped TiO_2 thin films. *Appl. Catal. B-Environ.* **150–151**, 74–81.

Qin, Z. Z., Liu, Z. L., Zeng, Y. F., Sun, J. H. & Yang, K. D. 2009 The effects of different methods of catalyst preparation on the hydro-electric plasma TiO_2-catalyzed degradation of 2,4-dinitrophenol. *Environ. Chem. Lett.* **7**, 147–153.

Ren, F. Z., Li, H. Y., Wang, Y. X. & Yang, J. J. 2015 Enhanced photocatalytic oxidation of propylene over V-doped TiO_2 photocatalyst: reaction mechanism between V^{5+} and single-electron-trapped oxygen vacancy. *Appl. Catal. B-Environ.* **176–177**, 160–172.

Sangari, M., Umadevi, M., Mayandi, J. & Pinheiro, J. P. 2015 Photocatalytic degradation and antimicrobial applications of F-doped MWCNTs/TiO_2 composites. *Spectrochim. Acta. A Mol. Biomol. Spectrosc.* **139**, 290–295.

Schneider, J., Matsuoka, M., Takeuchi, M., Zhang, J. L., Horiuchi, Y., Anpo, M. & Bahnemann, D. W. 2014 Understanding TiO_2 photocatalysis: mechanisms and materials. *Chem. Rev.* **114**, 9919–9986.

Snyder, H. R. & Anderson, G. K. 2001 Effect of air and oxygen content on the dielectric barrier discharge decomposition of chlorobenzene. *IEEE Trans. Plasma Sci.* **37**, 959–964.

Tang, S. F., Lu, N., Li, J., Shang, K. F. & Wu, Y. 2013 Improved phenol decomposition and simultaneous regeneration of granular activated carbon by the addition of a titanium dioxide catalyst under a dielectric barrier discharge plasma. *Carbon* **53**, 380–390.

Wang, Y. Q., Cheng, H. M., Hao, Y. Z., Ma, J. M., Li, W. H. & Cai, S. M. 1999 Photoelectrochemical properties of metal-ion-doped TiO_2 nanocrystalline electrodes. *Thin Solid Films* **349**, 120–125.

Wang, J., Zhao, Y. F., Wang, T., Li, H. & Li, C. 2015 Photonic, and photocatalytic behavior of TiO_2 mediated by Fe, CO, Ni, N doping and co-doping. *Physica. B* **478**, 6–11.

Yamashita, H., Honda, M., Harada, M., Ichihashi, Y., Anpo, M., Hirao, T., Itoh, N. N. & Iwamoto, N. 1998 Preparation of titanium oxide photocatalysts anchored on porous silica glass by a metal ion-implantation method and their photocatalytic reactivities for the degradation of 2-propanol diluted in water. *J. Phys. Chem. B* **102**, 10707–10711.

Yan, X. B., Tay, B. K. & Yang, Y. 2006 Dispersing and functionalizing multiwalled carbon nanotubes in TiO_2 sol. *J. Phys. Chem. B* **110**, 25844–25849.

Zhang, Y. Z., Deng, S. H., Sun, B. Y., Xiao, H., Li, L., Yang, G., Hui, Q., Wu, J. & Zheng, J. T. 2010 Preparation of TiO_2-loaded activated carbon fiber hybrids and application in a pulsed discharge reactor for decomposition of methyl orange. *J. Colloid. Interface Sci.* **347**, 260–266.

Zhang, Y., Xin, Q., Cong, Y. Q., Wang, Q. & Jiang, B. Q. 2013a Application of TiO_2 nanotubes with pulsed plasma for phenol degradation. *Chem. Eng. J.* **215–216**, 261–268.

Zhang, Y., Lu, J. N., Wang, X. P., Xin, Q., Cong, Y. Q., Wang, Q. & Li, C. J. 2013b Phenol degradation by TiO_2 photocatalysts combined with different pulsed discharge systems. *J. Colloid. Interface. Sci.* **409**, 104–111.

Zhang, M., Lu, D. D., Zhang, Z. H. & Yang, J. J. 2014 Enhancement of visible-light-induced photocurrent and photocatalytic activity of V and N codoped TiO_2 nanotube array films. *J. Electrochem. Soc.* **161**, 416–421.

Zhang, H., Sun, X. Q., Wang, Y. W. & Xu, X. X. 2019 Switching on wide visible light photocatalytic activity over $Mg_4Ta_2O_9$ by nitrogen doping for water oxidation and reduction. *J. Catal.* **377**, 455–464.

Zhong, J. S., Xu, J. R. & Wang, Q. Y. 2014 Nitrogen and vanadium co-doped TiO_2 mesosponge layers for enhancement in visible photocatalytic activity. *App. Surf. Sci.* **315**, 131–137.

First received 13 October 2020; accepted in revised form 23 November 2020. Available online 7 December 2020